# The effects of shape and flexibility on bio-engineered fd-virus suspensions

M. Dennison, M. Dijkstra, and R. van Roij

Citation: J. Chem. Phys. **135**, 144106 (2011); doi: 10.1063/1.3646951
View online: http://dx.doi.org/10.1063/1.3646951
View Table of Contents: http://jcp.aip.org/resource/1/JCPSA6/v135/i14
Published by the American Institute of Physics.

# The effects of shape and flexibility on bio-engineered fd-virus suspensions

M. Dennison,[1,a)] M. Dijkstra,[1] and R. van Roij[2]
[1]*Soft Condensed Matter, Debye Institute for Nanomaterials Science, Utrecht University, Princetonplein 5, 3584 CC Utrecht, The Netherlands*
[2]*Institute for Theoretical Physics, Utrecht University, Leuvenlaan 4, 3584 CE Utrecht, The Netherlands*

(Received 5 July 2011; accepted 16 September 2011; published online 11 October 2011)

We present a theoretical model to describe binary mixtures of semi-flexible rods, applied here to fd-virus suspensions. We investigate the effects of rod stiffness on both monodisperse and binary systems, studying thick-thin and long-short mixtures. For monodisperse systems, we find that fd-virus particles have to be made extremely stiff to even approach the behavior of rigid rods. For thick-thin mixtures, we find increasingly rich phase behavior as the rods are either made more flexible or if their diameter ratio is increased. For long-short rod mixtures we find that the phase behavior is controlled by the relative stiffness of the rods, with increasing the stiffness of the long rods or decreasing that of the short rods resulting in richer phase behavior. We also calculate the state point dependent effective shape of the rods. The flexible rods studied here always behave as shorter, thicker rigid rods, but with an effective shape that varies widely throughout the phase diagrams, and plays a key role in determining phase behavior. © *2011 American Institute of Physics*. [doi:10.1063/1.3646951]

## I. INTRODUCTION

In his seminal paper on nematic liquid crystals,[1] Onsager demonstrated that the transition from an isotropic (I) to a nematic (N) phase can be driven by entropic effects alone. Specifically, Onsager showed how the I-N phase transition of very long and thin hard rods can be explained by the competition between entropy arising from the mixing of particles of differing orientations, and that arising from excluded volume effects which are expressed via the virial coefficients.

Truncated at second virial order, Onsager theory is exact for infinitely long, rigid hard rods. However, for more realistic particles a more generalized approach is required. For instance, to accurately describe more spherical particles, such as spheroids[2–4] or cut-spheres,[5] higher order virial coefficients must either be included explicitly or approximated in some way. For very long rod-like particles, where the second virial approximation may be valid, it is often the case that the particles to be studied are not rigid, but instead are semi-flexible.

Introducing flexibility to models of rod-like particles can be done using a number of methods. Khokhlov and Semenov[6,7] used an excluded volume driven model to describe the nematic ordering in semi-flexible worm-like chains. The chain may flex in a continuous and uniform manner, with a stiffness that is characterized by the persistence length. Khokhlov and Semenov showed that only a slight flexibility is needed to significantly increase the coexistence densities of the I-N phase transition, later confirmed by simulation results.[8] However, the continuous nature of the chain makes the model mathematically somewhat complex, and as such the predictions obtained by Khokhlov and Semenov were in the limits where finite size effects were assumed to be negligible. These predictions were later confirmed by Chen,[9] who exactly solved the Khokhlov-Semenov model by discretizing the continuous chain.

Evans[10] introduced a bendable ellipsoid model, where the bending amplitude can be related to the persistence length. This model had the advantage of offering a complete analytic density-functional solution, although only when the ellipsoids remain convex, limiting the study to relatively small degrees of flexibility. However, the study showed the same behavior as Refs. 6 and 7, with an increase in the bending amplitude (decrease in stiffness) resulting in an increase in the coexistence densities. Also observed was the stretching of particles in the nematic phase as density was increased.

Ultimately, theories of semi-flexible rods that wish to study non-convex behavior rely on discretizing the flexibility to some extent. For instance, one may split the rod into segments of length equal to the persistence length $P$, which is the length over which the particle orientation remains correlated, and consider the rod as rigid over this length, although such a simple approximation is rarely valid and often requires reformulating.[11] An appealing model, which offers a fully discrete description of particle flexibility, was given by Wessels and Mulder,[12,13] who described a semi-flexible rod as a chain of connected, identical rigid-rod segments. Flexibility is incorporated in the model by introducing a bending potential between chain segments, and the excluded volume of the chain is considered at the segment level. The bending potential gives rise to a stiffness of the rod, characterized by its persistence length. This approach reproduces (within the continuum limit) the results of Refs. 6 and 7. The advantage of this model is that only a discrete number of degrees of freedom has to be considered, such that explicit calculations of extensions to binary systems are possible.[14]

Binary mixtures have long been used as a first-step generalization of liquid crystalline theory towards describing polydispersity. In addition to the orientational and excluded volume interaction entropies present for monodisperse

a)Author to whom correspondence should be addressed. Electronic mail: m.j.dennison@uu.nl.

 

systems, an additional mixing entropy is now included,[15,16] leading to increasingly rich phase behavior. For thick-thin rigid rod mixtures, for instance, the phase behavior predicted theoretically[16] and observed using simulations[17] includes I-N coexistence with strong fractionation effects, N-N and I-I demixing regimes, and I-I-N and I-N-N triple points. The observed phase behavior is strongly dependent on the diameter ratio $d$ of the rods, with mixtures with small $d$ exhibiting only I-N coexistence. Increasing $d$ shows the emergence of a N-N demixing regime, emerging from an I-N-N triple point and ending in a high-density (*upper*) critical point. Increasing $d$ still further leads to the emergence of an I-I demixing regime, beginning from a low-density (*lower*) critical point and ending in an I-I-N triple point.

Long-short rigid rod mixtures show much the same phase behavior,[15,18–21] with simple phase diagrams showing only I-N coexistence for small length ratios $q$, to complex diagrams with I-N, N-N, and I-N-N coexistence at large length ratios, with experimental observations showing the same qualitative phase behavior as predicted theoretically.[22] Long-short mixtures have also been studied both theoretically[11] and experimentally[23] for semi-flexible polymers, although only for a restricted persistence length range. Experimentally, the observed phase behavior was qualitatively the same as that observed for rigid rods, although the theoretical model of Ref. 11 failed to predict I-N-N and N-N coexistence. No I-I demixing has been reported in these long-short systems.[21]

A study by Purdy *et al.* gave the first experimental results for thick-thin binary colloidal rod mixtures.[24] The system consisted of fd-virus particles, which are charged and semi-flexible needles with a contour length $L = 880$ nm, a length-to-diameter ratio ($L/D$) exceeding 100, and a persistence length $P = 2.5\ L$, often used as model systems of colloidal rods due to their long, thin shape and low polydispersity. In a monodisperse system the fd-virus exhibits isotropic, nematic, smectic, columnar, and crystalline phases upon increasing the concentration.[25–27] By coating particles with a polymer, polyethylene-glycol (PEG), systems of bare and PEG-coated fd-virus particles were used to give mixtures with diameter ratios of $d = 1.1 - 3.7$. The study showed much the same phase behavior as predicted theoretically on the basis of the rigid rod model[16] (with an absence of I-I and I-I-N regions due to the limited diameter ratio range). However, the N-N demixing range observed showed a lower critical point that shifts to lower densities with increasing $d$, in contrast to the upper critical point found in Ref. 16. A rescaled Onsager theory, which approximated the higher order virial coefficients using the Parsons-Lee method,[28,29] gave qualitative agreement with these experimental results,[24,30] predicting the observed lower critical point of the N-N demixing range, but only by making assumptions about the shape of the rods: in order for this model system of rigid rods to fully capture the qualitative phase behavior of the binary fd-virus systems, much shorter, thicker rods had to be used, with the PEG coated fd-virus found to require $L/D \lesssim 7$, much lower than the true values.[24,30] The inference is that long semi-flexible rods exhibit the same phase behavior as short rigid rods due to the equivalent excluded volumes.[31,32] Quantitatively, this rigid rod model overestimates the diameter ratios at which the various phase separations are found. For instance, the experiments show N-N demixing to be present for diameter ratios as low as $d \gtrsim 2 - 3$, while the rigid-rod models predict $d \gtrsim 4 - 5$.[24,30] In a recent publication, we demonstrated that the key to a real understanding of these systems is flexibility, which renders the rods effectively shorter and thicker, avoids having to make explicit assumptions about their shape, *and* gives excellent qualitative and quantitative agreement with experimental observations.[14] In this paper, our purpose is twofold: (i) to give a complete description of the method used in Ref. 14, and (ii) to explore the effects of flexibility on both monodisperse and bidisperse fd-virus systems with different diameter (thick-thin) and length (long-short) ratios. This is achieved by altering the fd-virus stiffness, via changing the persistence length, which has recently been shown to be possible experimentally,[33] with persistence lengths ranging from $2.5\ L$ to $\sim 10\ L$. We also define and calculate an effective shape for the particles, which allows us to look at how they stretch throughout the systems we study.

The structure of the paper is as follows. In Sec. II we generalize the segmented chain model of Wessels and Mulder[12,13] to describe binary systems of semi-flexible rods, and define the effective shape of the particles. In Sec. III we apply this model to monodisperse fd-virus suspensions of different persistence lengths. In Sec. IV we apply the model to the binary fd-virus systems studied in Ref. 24, looking at an expanded diameter ratio range than the experiments and also looking at the effects of particle stiffness on phase behavior. In addition, we study long-short fd-virus mixtures. Finally, we present our conclusions in Sec. V.

## II. THEORY

We consider a suspension of $N_i$ semi-flexible rods of species $i = 1, 2$ with contour lengths $L_i$, in a volume $V$ at temperature $T$. We follow Wessels and Mulder,[12,13] and model a rod of species $i$ as a chain of $M_i$ rod-like segments of length $l_i = L_i/M_i$ and diameter $D_i \ll l_i$. Connected chain segments have a bending energy given by

$$u_i(\omega_m, \omega_{m+1}) = -\frac{P_i}{l_i}\omega_m \cdot \omega_{m+1}, \tag{1}$$

where the orientation of the $m$th segment is given by the unit-vector $\omega_m$ (with $1 \le m \le M_i$) and $P_i$ is the persistence length which describes the stiffness of the chain.[12,13] We use thermal energy units by setting $\beta = 1/k_BT = 1$. The total bending potential of a chain of species $i$ with orientation $\mathbf{\Omega} = \{\omega_1, \ldots, \omega_{M_i}\}$ is then given as

$$U_i(\mathbf{\Omega}) = \sum_{m=1}^{M_i-1} u_i(\omega_m, \omega_{m+1}). \tag{2}$$

The Helmholtz free energy of the suspension, $F$, consists of four key parts: the translational and mixing ideal-gas contributions, the orientation entropy, the bending energy, and the excluded volume interactions. The variational free-energy functional $F[f_1, f_2]$ of the system within an Onsager-like

second virial approximation is therefore given as

$$\frac{F}{N} = \ln(B\rho) - 1 + x_1 \ln x_1 + x_2 \ln x_2 + \sum_{i=1}^{2} x_i \int f_i(\mathbf{\Omega})(\ln(4\pi f_i(\mathbf{\Omega})) + U_i(\mathbf{\Omega}))d\mathbf{\Omega} + \frac{\rho}{2}\sum_{i,j=1}^{2} x_i x_j \int f_i(\mathbf{\Omega}) f_j(\mathbf{\Omega}')K_{ij}(\mathbf{\Omega}, \mathbf{\Omega}')d\mathbf{\Omega}d\mathbf{\Omega}', \tag{3}$$

where $N = N_1 + N_2$ is the total number of rods, $\rho = N/V$ is the number density, $B = \pi D_1 L_1^2/4$ is a constant, $x_i = N_i/N$ defines the composition of the mixture (with $x_1 = 1 - x_2$), and $f_i(\mathbf{\Omega})$ is the orientation distribution function (ODF) of species $i$, which satisfies the normalization $\int d\mathbf{\Omega} f_i(\mathbf{\Omega}) = 1$ where $d\mathbf{\Omega} = \prod_{m=1}^{M_i} d\omega_m$. The excluded volume interaction between species $i$ and $j$ is given by[12,13]

$$K_{ij}(\mathbf{\Omega}, \mathbf{\Omega}') = \sum_{m=1}^{M_i}\sum_{m'=1}^{M_j} k_{ij}(\omega_m, \omega_{m'}), \tag{4}$$

where $k_{ij}(\omega_m, \omega_{m'})$ is the excluded volume between segment $m$ of species $i$ and segment $m'$ of species $j$, which is given by

$$k_{ij}(\omega_m, \omega_{m'}) = l_i l_j (D_i + D_j)|\sin\gamma(\omega_m, \omega_{m'})|, \tag{5}$$

where $\gamma(\omega_m, \omega_{m'}) = \arccos(\omega_m \cdot \omega_{m'})$ is the angle between chain segments $m$ and $m'$. Equation (3) is a two-component generalization of the one-component segmented-chain functional of Refs. 12 and 13. In the case of $M_1 = M_2 = 1$ and $U_1 = U_2 \equiv 0$, it reduces to the Onsager functional for binary mixtures of rigid rods,[15,16] while for $M_1 = M_2 = 1$, $U_1 = U_2 \equiv 0$, and identical species $1 = 2$, it reduces to the standard Onsager Helmholtz free energy.[1]

The equilibrium ODFs minimize $F$ subject to the normalization constraints, and must therefore satisfy the nonlinear self consistent equation

$$f_i(\mathbf{\Omega}) = \frac{\exp(-U_i(\mathbf{\Omega}) - V_i(\mathbf{\Omega}))}{Q_i}, \tag{6}$$

where $Q_i$ is a partition function-like normalization factor arising from the normalization condition $\int d\mathbf{\Omega} f_i(\mathbf{\Omega}) = 1$, and $V_i(\mathbf{\Omega})$ can be seen as a self-consistent field, arising from the excluded volume interactions, acting on all segments of a chain, given as

$$V_i(\mathbf{\Omega}) = \rho \sum_{j=1}^{2} x_j \int K_{ij}(\mathbf{\Omega}, \mathbf{\Omega}') f_j(\mathbf{\Omega}')d\mathbf{\Omega}'. \tag{7}$$

Although it is, in principle, possible to explicitly solve Eqs. (6) and (7) for a given state point numerically, this calculation is not very efficient for a large number $M$ of segments. Instead, it turns out to be much more efficient to calculate the ODFs at the segment level. We denote the ODF of the $m$th segment ($m = 1, \ldots, M_i$) of a chain of species $i = 1, 2$ as $f_{i,m}(\omega_m)$, which is defined by

$$f_{i,m}(\omega_m) = \int f_i(\mathbf{\Omega})d\omega_1 \ldots d\omega_{m-1}d\omega_{m+1} \ldots d\omega_{M_i}, \tag{8}$$

where we are integrating out all degrees of freedom from $f_i(\mathbf{\Omega})$ *except* those of the $m$th segment. Inserting Eq. (6) into Eq. (8), and evaluating, gives us

$$f_{i,m}(\omega_m) = \frac{1}{Q_i} q_{i,m}(\omega_m)\exp[-v_i(\omega_m)]q_{i,M-m+1}(\omega_m), \tag{9}$$

where $v_i(\omega)$ is given by expressing Eq. (7) at the segment level by combining Eq. (4) with Eq. (7) to give $V_i(\mathbf{\Omega}) = \sum_{m=1}^{M_i} v_i(\omega_m)$, with $v_i(\omega)$ being the same self-consistent field

$$v_i(\omega_m) = \rho \sum_{j=1}^{2}\sum_{m'=1}^{M_j} x_j \int k_{ij}(\omega_m, \omega_{m'}) f_{j,m'}(\omega_{m'})d\omega_{m'}, \tag{10}$$

acting on all segments of a chain of species $i$. The factor $q_{i,m}(\omega_m)$ is the partial-chain partition function of segment $m$, given by

$$q_{i,m}(\omega_m) = \int \prod_{n=1}^{m-1} \exp[-v_i(\omega_n) - u_i(\omega_n, \omega_{n+1})]d\omega_n, \tag{11}$$

which can be rewritten as the recursion relation:

$$q_{i,m}(\omega_m) = \int d\omega_{m-1} q_{i,m-1}(\omega_{m-1}) \times \exp[-v_i(\omega_{m-1}) - u_i(\omega_{m-1}, \omega_m)]. \tag{12}$$

Due to the normalization of $f_{i,m}(\omega_m)$, we may arbitrarily choose $q_{i,1}(\omega_1) = 1$, from which the recursion relation can be started.

At a given state point, $f_{i,m}(\omega_m)$ is then calculated as follows. We choose an initial guess for $v_i(\omega_m)$, from which we may calculate $q_{i,m}(\omega_m)$ for $m = 2, \ldots, M_i$ from Eq. (12) and $q_{i,1}(\omega_1) = 1$. We use these to calculate $f_{i,m}(\omega_m)$ and $Q_i$ from Eq. (9), from which $v_i(\omega_m)$ is recalculated from Eq. (10). The new $v_i(\omega_m)$ is then reinserted into Eq. (12) to calculate $q_{i,m}(\omega_m)$ for $m = 2, \ldots, M_i$, and the process is repeated until convergence is found. The equilibrium free energy is then given by

$$\frac{F_{\text{eq}}}{N} = \ln(B\rho) - 1 + x_1 \ln\frac{x_1}{Q_1} + x_2 \ln\frac{x_2}{Q_2} - \frac{1}{2}\rho \sum_{i,j}^{2} x_i x_j \sum_{m=1}^{M_i}\sum_{m'=1}^{M_j} \times \int k_{ij}(\omega_m, \omega_{m'}) f_{i,m}(\omega_m) f_{j,m'}(\omega_{m'})d\omega_m d\omega_{m'}. \tag{13}$$

We note that as we are studying uniaxial particles and phases that the ODFs are only dependent on the polar angle $\theta$ of $\omega$ with respect to the nematic director, such that the azimuthal angle $\phi$ may be accounted for in advance of the calculations. For example, functions dependent on only a single orientation $\omega$, such as the ODFs, simply become $f_{i,m}(\omega_m) = f_{i,m}(\theta_m)$. Functions dependent on two orientations, such as the excluded volume interactions $k_{ij}(\omega_m, \omega_{m'})$, may also be integrated over the azimuthal angles prior to the main calculations. This involves a new excluded volume term

$k'_{ij}(\theta_m, \theta_{m'})$, which is given by

$$k'_{ij}(\theta_m, \theta_{m'}) = \int_0^{2\pi} d\phi_m \int_0^{2\pi} d\phi_{m'} k_{ij}(\omega_m, \omega_{m'}). \tag{14}$$

Due to this azimuthal symmetry, and after performing these integrations prior to the main calculation, we only need to consider an angular grid for $\theta$, which due to the up-down symmetry of the rods considered in this work reduces to a grid for the polar angle in the range $\theta \in (0, \pi/2)$. We then use simple numerical integration to evaluate all integrals.

With the ODFs known, $F_{\text{eq}}$ may be calculated from Eq. (13). From this, all other thermodynamic properties follow. The osmotic pressure $\Pi$ is calculated from

$$\Pi = \rho^2 \frac{\partial(F_{\text{eq}}/N)}{\partial \rho}, \tag{15}$$

while the Gibbs free energy per particle $\tilde{g}$ is given by

$$\tilde{g}(x, \Pi) = \frac{F_{\text{eq}}}{N} + \frac{\Pi}{\rho}. \tag{16}$$

We locate coexisting phases by fixing $\Pi$ and calculating $\tilde{g}$ as a function of $x_2$, in both the isotropic and nematic phases, and then performing common tangent constructions.[16,34,35]

We may also calculate the nematic order parameters $S_i$ of the rods. We start by defining the local order of the $m$th segment $S_{i,m}$ as

$$S_{i,m} = \int d\omega_m f_{i,m}(\omega_m) P_2(\omega_m \cdot \mathbf{n}), \tag{17}$$

where $P_2(\omega_m \cdot \mathbf{n})$ is the second Legendre polynomial, and $\mathbf{n}$ is the nematic director. As before, we only need to consider the polar dependence of the particle orientation, and this therefore becomes

$$S_{i,m} = 4\pi \int_0^{\pi/2} d\theta_m f_{i,m}(\theta_m) P_2(\cos\theta_m), \tag{18}$$

where we define $\mathbf{n}$ to be along the $z$ axis, such that $\omega_m \cdot \mathbf{n} = \cos\theta_m$. The total nematic order of a rod is defined as the average nematic order along the chain, given as

$$S_i = \frac{1}{M_i} \sum_{m=1}^{M_i} S_{i,m}. \tag{19}$$

The calculation of the effective length goes as follows. We define the mean square effective length $L^2_{e,i}$ as

$$\begin{aligned} L^2_{e,i} &= l_i^2 \sum_{m=1}^{M_i} \sum_{m'=1}^{M_i} \langle \omega_m \cdot \omega_{m'} \rangle \\ &= l_i^2 \sum_{m=1}^{M_i} \sum_{m'=1}^{M_i} \int (\omega_m \cdot \omega_{m'}) \\ &\quad \times f_{i,m,m'}(\omega_m, \omega_{m'}) d\omega_m d\omega_{m'}, \end{aligned} \tag{20}$$

where we are summing the squares of the average length projections of all chain segments $m'$ along the director of all segments $m$. Here, $f_{i,m,m'}(\omega_m, \omega_{m'})$ is the pair orientational distribution function (PDF) defined by

$$f_{i,m,m'}(\omega_m, \omega_{m'}) = \int f_i(\mathbf{\Omega}) \delta(\omega_m - \omega) \delta(\omega_{m'} - \omega') d\mathbf{\Omega}, \tag{21}$$

where we are integrating out all degrees of freedom from $f_i(\mathbf{\Omega})$ except those of segments $m$ and $m'$. Note that $f_{i,m,m'}(\omega_m, \omega_{m'})$ is the probability that a chain of species $i$ is in a configuration with the $m$th and $m'$th segments having orientations $\omega_m$ and $\omega_{m'}$, simultaneously. Inserting Eq. (6) into Eq. (21), and using Eqs. (10) and (11), we find that

$$\begin{aligned} f_{i,m,m'}(\omega_m, \omega_{m'}) &= \frac{1}{Q_i} q_{i,m}(\omega_m) \exp[-v_i(\omega_m)] \\ &\quad \times Q_{i,m,m'}(\omega_m, \omega_{m'}) \exp[-v_i(\omega_{m'})] \\ &\quad \times q_{i,M-m'+1}(\omega_{m'}), \end{aligned} \tag{22}$$

with the same notation as before. Here, $Q_{i,m,m'}(\omega_m, \omega_{m'})$ is the partial chain partition function that takes into account the effect of the chain segments that link segment $m$ and segment $m'$. For neighboring segments, $m' = m + 1$, we have $Q_{i,m,m'}(\omega_m, \omega_{m'}) = \exp[-u_i(\omega_m, \omega_{m'})]$, and for $m' = m + 2, \ldots, M_i$, it follows the recursion relation

$$\begin{aligned} Q_{i,m,m'}(\omega_m, \omega_{m'}) &= \int d\omega_{m'-1} Q_{i,m,m'-1}(\omega_m, \omega_{m'-1}) \\ &\quad \times \exp[-v_i(\omega_{m'-1})] \\ &\quad \times \exp[-u_i(\omega_{m'-1}, \omega_{m'})]. \end{aligned} \tag{23}$$

By construction, each pair orientation distribution function also obeys the normalization condition $\int f_{i,m,m'}(\omega_m, \omega_{m'}) d\omega d\omega_{m'} = 1$. As we already know the ODFs, and hence $q_{i,m}(\omega_m)$ and $v_i(\omega_m)$, from our phase diagram calculations, the calculation of the PDFs and $L_{e,i}$ is relatively straightforward. We use $L_{e,i}$ to calculate the effective diameter $D_{e,i}$, which we define as the diameter required for rigid rods to have the same excluded volume as our semi-flexible rods at the same state point. We calculate this by equating the excluded volume of species $i$ (calculated in Eq. (13)) to that of a system of rigid rods of length $L_{e,i}$ with the same composition $x_2$ and at the same nematic order parameter $S$, such that

$$\begin{aligned} &l_i^2 D_i \sum_{m=1}^{M_i} \sum_{m'=1}^{M_i} \int f_{i,m}(\omega_m) f_{i,m'}(\omega_{m'}) \\ &\times |\sin\gamma(\omega_m, \omega_{m'})| d\omega_m d\omega_{m'} \\ &\quad = L^2_{e,i} D_{e,i} \int f_i(\mathbf{\Omega}) f_i(\mathbf{\Omega}') |\sin\gamma(\mathbf{\Omega}, \mathbf{\Omega}')| d\mathbf{\Omega} d\mathbf{\Omega}'. \end{aligned} \tag{24}$$

The top two lines are the excluded volume of a system of semi-flexible rod of species $i$, as calculated in Eq. (13). The bottom line is the excluded volume of a system of rigid rods of length $L_{e,i}$, with the same composition $x_2$ and at the same nematic order parameter $S$ as the semi-flexible rods. To solve this, we initially evaluate the integral for a range of order parameters $S$, producing a lookup table from which we extract the value that corresponds to the $S$ value of the flexible rod system via spline interpolation. This leaves $D_{e,i}$ as the only

unknown in Eq. (24), and we then obtain the effective shape of the rods $L_{e,i}/D_{e,i}$. We express this as a fraction of the actual shape by

$$(L_{e,i}/D_{e,i})^* = \frac{L_{e,i}/D_{e,i}}{L_i/D_i}. \quad (25)$$

## III. MONODISPERSE SYSTEMS

In this section, we examine the behavior of monodisperse fd-virus suspensions for a range of persistence lengths. We keep the contour length fixed at $L = 0.88\ \mu$m and the diameter at $D = 6.6$ nm,[24] and vary the persistence length $P$.

It is first important to check that the segment chain model is within the continuum limit of semi-flexible rods. That is, we must ensure that we use a sufficiently large number of chain segments $M$ such that our results capture the physics of a continuous chain. We therefore examine the convergence of our results with increasing $M$. In Fig. 1(a) we show the equations of state (EOS) of both the I and N phases of a one-component bare-fd-virus system, with the unmodified fd-virus persistence length $P = 2.5\ L = 2.2\ \mu$m. We observe that for all $M$ values the isotropic EOS is the same, while the nematic branch and I-N coexistence densities differ. Using $M = 1$ chain segment, corresponding to a rigid rod, gives the lowest coexistence densities and pressure (with isotropic density $\rho_I B = 3.29$, nematic density $\rho_N B = 4.19$, and coexistence pressure $\beta\Pi_{IN}B = 14.12$), and a nematic branch of the EOS that is significantly below the other results. Increasing $M$ gives progressively higher values of the coexistence densities and nematic EOS, until we see convergence beyond $M \sim 11$. As such, we use $M = 15$ chain segments for all unmodified fd-virus particles, for which we find the isotropic-nematic coexistence properties to be $\rho_I B = 4.96$, $\rho_N B = 5.44$, and $\beta\Pi_{IN}B = 29.55$. For more flexible particles with lower persistence lengths, more chain segments must be used to find convergence. This is illustrated in Fig. 1(b), where for $P = 1.1\ \mu$m we see convergence only beyond $M \sim 20$, and hence we use $M = 22$ in our calculations. We find the coexistence properties to be $\rho_I B = 6.74$, $\rho_N B = 7.26$, and $\beta\Pi_{IN}B = 52.21$, a significant shift from those of the unmodified fd-virus.

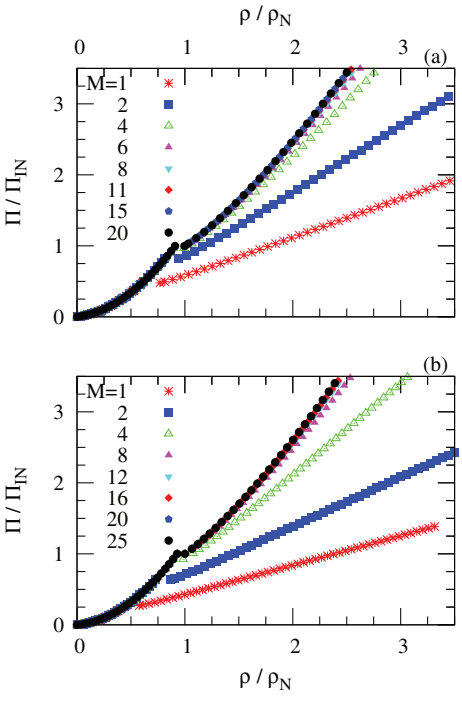


FIG. 1. Convergence of equation of state in $\rho/\rho_N - \Pi/\Pi_{IN}$ representation (with $\rho_N$ being the "converged" nematic coexistence density and $\Pi_{IN}$ being the coexistence pressure, using (a) $M = 15$ and (b) $M = 22$ chain segments), for increasing number of chain segments $M$ for fd-virus parameters $L = 0.88\ \mu$m and $D = 6.6$ nm with (a) $P = 2.2\ \mu$m ($\rho_I B = 4.96$, $\rho_N B = 5.44$, and $\beta\Pi_{IN}B = 29.55$ at coexistence, using $M = 15$) and (b) fd-virus with $P = 1.1\ \mu$m ($\rho_I B = 6.74$, $\rho_N B = 7.26$, and $\beta\Pi_{IN}B = 52.21$ at coexistence, using $M = 22$).

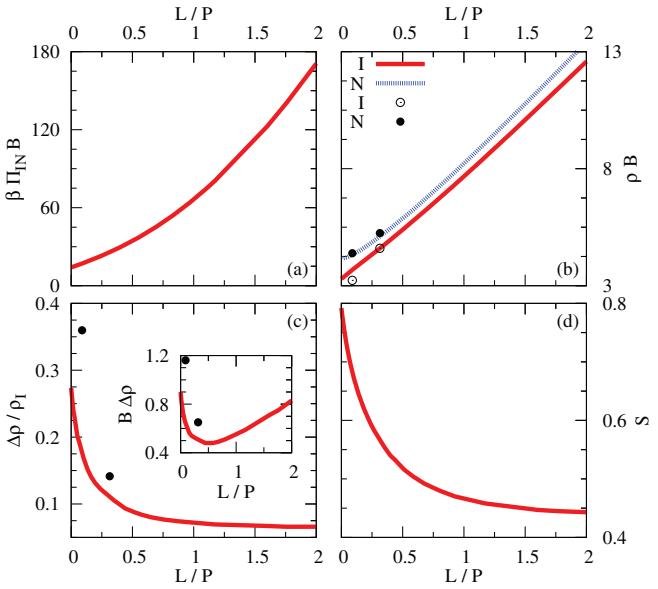


FIG. 2. Properties of fd-virus suspension ($L = 0.88\ \mu$m and $D = 6.6$ nm) of a range of persistence lengths $P$ at isotropic-nematic coexistence. (a) Coexistence osmotic pressure $\Pi_{IN}$, (b) coexistence densities $\rho_I$ and $\rho_N$, (c) jump in density at coexistence $\Delta\rho = \rho_N - \rho_I$ (normalized and unnormalized (inset) by $\rho_I$), and (d) nematic order parameter $S$. Points show experimental data of Ref. 33.

We now examine the behavior of the suspensions at I-N coexistence. Figure 2 shows the osmotic pressure at coexistence ($\Pi_{IN}$), the isotropic and nematic coexistence densities ($\rho_I$ and $\rho_N$, respectively), the jump in density at coexistence $\Delta\rho = \rho_N - \rho_I$, and the nematic order parameter $S$ at $\rho_N$ for fd-virus suspensions of a range of stiffnesses, ranging from rigid rods to fd-virus particles with $P = L/2 = 0.44\ \mu$m. Figures 2(a) and 2(b) show that, as one would expect, the pressure and coexistence densities increase greatly as the fd-virus is made more flexible, qualitatively consistent with the theoretical results of Refs. 6, 7, 9–13 and the simulation results of Ref. 8. Comparing our predicted coexistence densities to the experimental data of Ref. 33 (which we scale from concentrations to the dimensionless units used here using the method in Ref. 14) also shows very good quantitative agreement. In Fig. 2(d) we see that the nematic order parameter behaves in the opposite manner, decreasing as the rods become more flexible. Interestingly, while the pressure and coexistence densities continue to increase drastically as $P$ is decreased, the decrease in the nematic order parameter appears to tail off. In

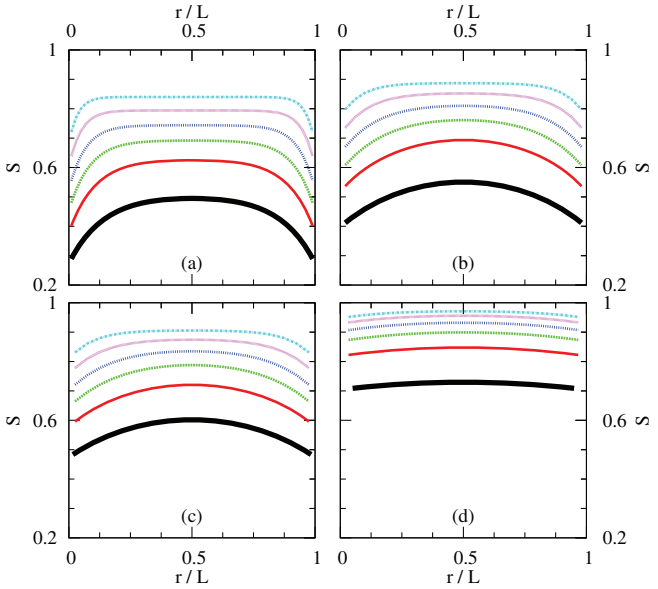


FIG. 3. Nematic order parameter $S$ of fd-virus particles ($L = 0.88$ $\mu$m and $D = 6.6$ nm) at various osmotic pressures $\Pi$, at a distance $r \in [0, L]$ along the rod. (a) $P = 0.44$ $\mu$m, (b) $P = 1.5$ $\mu$m, (c) $P = 2.2$ $\mu$m, and (d) $P = 17.6$ $\mu$m. The lowest line is for $\Pi$ at I-N coexistence ($\Pi_{IN}$), and higher lines are for $\Pi = 1.2$, 1.5, 2, 3, and $5\Pi_{IN}$, respectively.

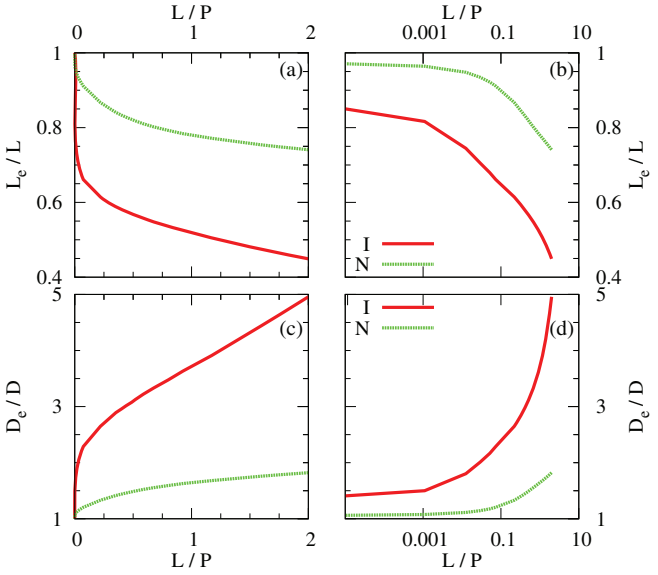


FIG. 4. Effective length $L_e$ ((a) on linear $L/P$ scale and (b) on logarithmic $L/P$ scale) and effective diameter $D_e$ ((c) on linear $L/P$ scale and (d) on logarithmic $L/P$ scale) of fd-virus (with contour length $L = 0.88$ $\mu$m and diameter $D = 6.6$ nm) suspension of a range of persistence lengths $P$ at I-N coexistence. Solid line shows results for isotropic phases, dashed line shows nematic phases.

Fig. 2(c) we show the jump in density at coexistence, showing both the absolute jump and the jump normalized by the isotropic coexistence density $\rho_I$. The normalized value, which is the jump in density as a fraction of the density at coexistence, shows similar behavior to the nematic order parameter, initially decreasing rapidly with $P$ before tailing off for small persistence lengths, showing that the transition becomes a progressively weaker first-order transition as the particles become more flexible. The absolute value behaves somewhat differently, showing a minimum at $L/P \sim 0.5$, which corresponds to fd-virus that is slightly more flexible than the unmodified fd-virus with $L/P = 0.4$. Comparing to experimental data,[33] we see our results underestimate the jump in density at coexistence, although they do match qualitatively.

Figures 3(a)–3(d) show the "local" nematic order parameter along the contour for fd-virus particles of a range of stiffnesses at various osmotic pressures $\Pi$. For the most flexible rods examined ($P = 0.44$ $\mu$m, shown in Fig. 3(a)), we see that at coexistence ($\Pi = \Pi_{IN}$), the innermost regions of the fd-virus are much more aligned along the nematic director than the outer segments, with the order parameter ranging from $S \sim 0.3$ to $S \sim 0.5$, with a single peak value at the very center of the rod. As $\Pi$ is increased we see that the difference in nematic ordering between the end segments and the center of the rods become progressively less dramatic, until at $\Pi = 5\Pi_{IN}$ we see $S$ ranging from $S \sim 0.72$ to $S \sim 0.84$. Interestingly, as $\Pi$ is increased, the peak value in the middle of the rod becomes a plateau, with more and more of the inner segments having the same $S$ values, and the less ordered end sections become shorter. As the particles are made stiffer they become increasingly more uniformly aligned, as expected, although for unmodified fd-virus (Fig. 3(c)) the difference is still quite pronounced, with $S$ values ranging from 0.48 to 0.6 at coexistence and 0.83 to 0.9 at $\Pi = 5\Pi_{IN}$.

We finally show results for the effective shape of fd and modified fd-virus systems. While the nematic order parameter $S$ along the contour (shown in Fig. 3) gives us an indication of the local stretching of the chain in the nematic phase, the effective shape allows us to look at this explicitly in both the isotropic and nematic phases. Figures 4(a) and 4(b) show the effective length $L_e$ and Figs. 4(c) and 4(d) show the effective diameter $D_e$ (defined in Eq. (20) and Eq. (24), respectively) in both the isotropic and nematic phases at coexistence, for fd-virus particles of a range of persistence lengths. In Figs. 4(a) and 4(c), we use a linear $L/P$ scale, while in Figs. 4(b) and 4(d), we use a logarithmic $L/P$ scale. As one would expect, we see shorter effective lengths and larger effective diameters for more flexible particles than for stiffer ones in both phases. This is particularly true of the isotropic phase, where we see $L_e \sim 0.45\ L$ and $L_e/D_e \sim 0.09\ L/D \sim 12$ for the most flexible particles studied ($P = L/2 = 0.44$ $\mu$m). Similar, but less extreme, results are obtained for unmodified fd-virus ($P = 2.5\ L = 2.2$ $\mu$m), which have $L_e \sim 0.6\ L$ and $L_e/D_e \sim 0.2\ L/D \sim 27$. Surprisingly, we see a sharp change in the $L/P$ dependence of the isotropic phase curves shown in Figs. 4(a) and 4(c) at high persistence lengths, with the effective shape increasing only gently with $P$ before approaching the actual shape rapidly after $P \sim 15\ L$. This indicates that it is necessary to increase the persistence length significantly before the effective shape of fd-virus in the isotropic phase begins to approach the actual shape, to a value of $P > 15\ L$, currently beyond experimental techniques for fd-virus particles.[36]

In the nematic phase, the behavior is similar but much less pronounced. In Fig. 4 we see $L_e \sim 0.75\ L$ and $L_e/D_e \sim 0.4\ L/D \sim 53$ for the most flexible fd-virus studied and $L_e \sim 0.83\ L$ and $L_e/D_e \sim 0.6\ L/D \sim 80$ for the unmodified fd-virus. The $L/P$ dependence of the curve as the particles

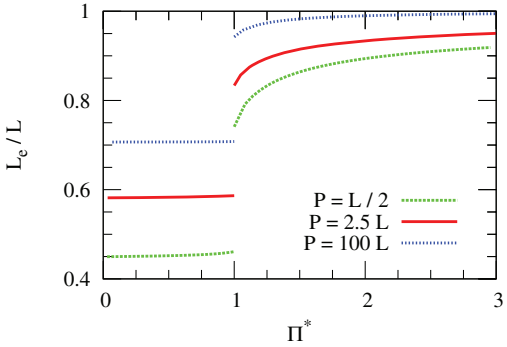


FIG. 5. Effective length $L_e$ of fd-virus particles ($L = 0.88$ $\mu$m and $D = 6.6$ nm) with varying persistence lengths $P$ as a function of osmotic pressure $\Pi^* = \Pi/\Pi_{IN}$, where $\Pi_{IN}$ is the pressure at coexistence ($\beta\Pi_{IN}B = 170.86$ for $P = L/2$, $\beta\Pi_{IN}B = 29.55$ for $P = 2.5\,L$, and $\beta\Pi_{IN}B = 14.49$ for $P = 100\,L$).

are made stiffer is also much smaller than in the isotropic phase, indicating that the excluded volume induced nematic ordering plays a stronger role in the straightening of the rods than increasing their stiffness.

In Fig. 5 we show the effective length of fd-virus particles for a range of persistence lengths as a function of osmotic pressure. Here, we track $L_e$ as the systems become denser. We find that for rods of large persistence length ($P = 100\,L$) the rods become effectively completely stretched at pressures just after coexistence, while for more flexible particles, including the unmodified fd-virus, the pressure must be increased far beyond coexistence for them to become completely stretched out. Such stretching of particles in the nematic phase was also observed in the bendable ellipsoid model of Ref. 10. We also note that even very stiff rods with $P = 100\,L$ are only slightly more stretched out in the isotropic phase than very flexible rods with $P = L/2$ are in the nematic phase at I-N coexistence, again showing how stiff the rods have to be made to become significantly stretched out in the isotropic phase.

## IV. BINARY MIXTURES

### A. Unmodified thick-thin fd-virus mixtures

In this section, we present phase diagrams for mixtures of bare-fd particles (species 1, thin) and PEG-coated ones (species 2, thick), with equal contour lengths $L_1 = L_2 = 0.88$ $\mu$m. We take the bare-fd diameter to be fixed at $D_1 = 6.6$ nm, and we study a range of diameter ratios $d = D_2/D_1$.[24] We begin by studying fd-virus particles with persistence lengths $P_1 = P_2 = 2.2$ $\mu$m, which is the standard value for unmodified fd-virus particles.[24] In Fig. 6 we show the phase diagrams, in the packing fraction representation $\eta_2 - \eta_1$, for diameter ratios $d = 1.2 - 6$. We distinguish between isotropic phases (I, with $f_{i,m}(\omega) = 1/4\pi$, a constant) and nematic phases (N, with $f_{i,m}(\omega)$ peaked about the nematic director, with the inner segments more so than those close to the chain ends, see Fig. 3).

For all $d$ studied we find I-N coexistence, with the I phase richer in thinner rods and the N phase richer in thicker rods, consistent with experimental observations.[24] For the smallest diameter ratio studied ($d = 1.2$, Fig. 6(a)), we see only

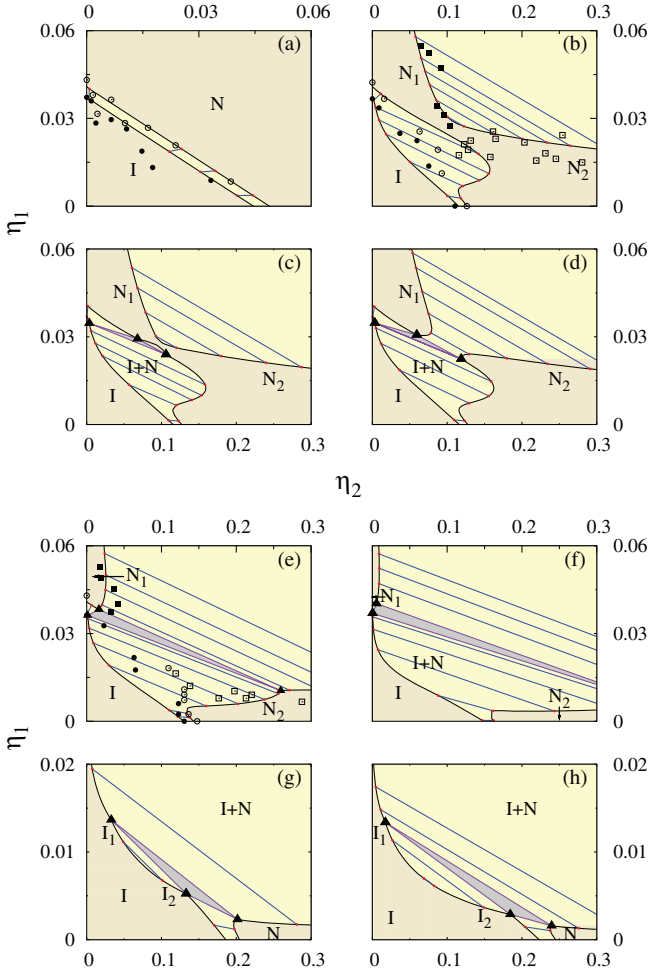


FIG. 6. Phase diagrams for mixtures of bare (thin) fd-virus particles (species 1) and PEG-coated (thick) ones (species 2) in the packing fraction representation $\eta_2 - \eta_1$, with $L_1 = L_2 = 0.88$ $\mu$m, $P_1 = P_2 = 2.2$ $\mu$m, $D_1 = 6.6$ nm, and diameter ratios $d = D_2/D_1 =$ (a) 1.2, (b) 3.1, (c) 3.11, (d) 3.125, (e) 3.5, (f) 4, (f) 5, and (h) 6. The lighter areas indicate the two-phase regions with tie-lines connecting coexisting state-points; triangles denote I-N-N and I-I-N triple points. Experimental results of Ref. 24 denoted by circles (I-N coexistence) and squares (N-N coexistence), for $d =$ (a) 1.1, (b) 2.9, and (e) 3.

this phase separation, and no N-N coexistence in the density regime of interest. Increasing $d$ leads to the emergence of a N-N demixing regime, which we first see for $d \sim 2.5$, consisting of one N phase rich in thinner rods and one richer in thicker rods. The N-N region begins from a lower critical point, and is separated from the I-N region by a single phase nematic region. We show this behavior for $d = 3.1$ in Fig. 6(b), and a similar phase diagram has been reported experimentally for $d = 2.9$.[24] If we increase $d$ slightly beyond this to 3.11 (Fig. 6(c)), we see the emergence of a second N-N demixing regime, which begins from an I-N-N triple point connected to the I-N coexistence region, and ends in an upper critical point. The initial N-N region beginning from a lower critical point is still present. Such phase behavior has not been reported experimentally, possibly because it is only found for a very small range of diameter ratios, and increasing $d$ to 3.125 (Fig. 6(d)) results in the two N-N demixing regions merging to form a single region, which begins from an I-N-N triple point and continues throughout the density range of interest here. This

phase behavior has been reported experimentally for $d \geq 3$,[24] and is found in our model for all $d$ values greater than 3.125, with the demixed N phases becoming increasingly monodisperse for increasing $d$ values. For $d$ values larger than $d \simeq 4.5$ we see the emergence of an I-I demixing regime, which begins from a lower critical point and ends in an I-I-N triple point, merging with the I-N region. Such phase behavior has previously been found for rigid rod mixtures with diameter ratios exceeding $d \simeq 8$,[16] but not yet in experimental systems where the largest diameter ratio studied has been $d = 3.7$.[24] We show this behavior for $d = 5$ and $d = 6$, noting that as $d$ is increased the I-I demixing region shows increasing fractionation.

We also make a quantitative comparison of our results to those found experimentally, using the method outlined in Ref. 14 to convert these from concentrations into packing fractions. We find very good agreement, particularly for low $d$ values, although we note that for larger diameter ratios we have to use a larger $d$ value in our theory than that used experimentally.

We now present results for the effective shape of bare and PEG-coated fd-virus particles for several of the binary mixtures studied above. Shown in Figs. 7(a)–7(c) is the

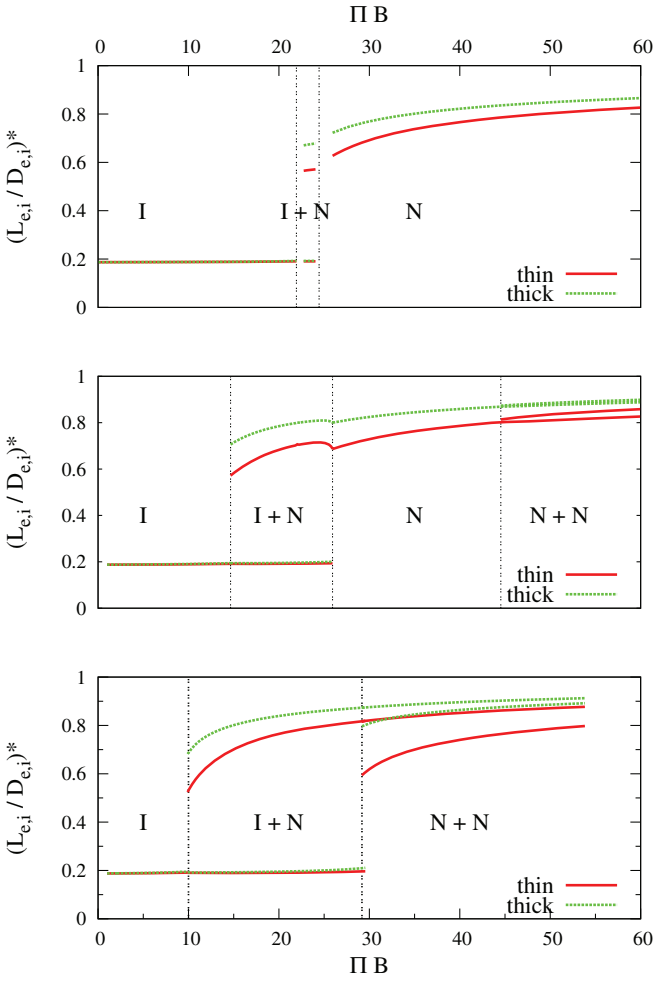


FIG. 7. Relative effective shape $(L_{e,i}/D_{e,i})^* = (L_{e,i}/D_{e,i})/(L_e/D_e)$ of thin (solid line) and thick (dashed line) rods with $L_1 = L_2 = 0.88\ \mu$m, $P_1 = P_2 = 2.2\ \mu$m, $D_1 = 6.6$ nm, and diameter ratios $d = D_2/D_1 =$ (a) 2, (b) 3, (c) 4, as a function of osmotic pressure $\Pi$ with mole fraction $x_2 = 0.25$ of thick rods.

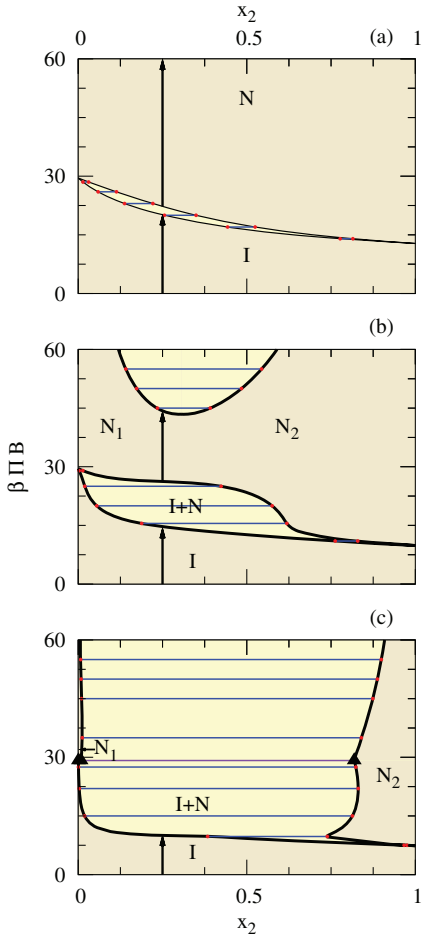


FIG. 8. Phase diagrams for mixtures of bare (thin) fd-virus particles (species 1) and PEG-coated (thick) ones (species 2) in the $x_2$-$\Pi$ representation, with $L_1 = L_2 = 0.88\ \mu$m, $P_1 = P_2 = 2.2\ \mu$m, $D_1 = 6.6$ nm, and diameter ratios $d = D_2/D_1 =$ (a) 2, (b) 3, and (c) 4. The lighter areas indicate the two-phase regions with tie-lines connecting coexisting state-points; triangles denote I-N-N and I-I-N triple points. The arrows show the path along $x_2 = 0.25$.

relative effective shape $(L_{e,i}/D_{e,i})^* = (L_{e,i}/D_{e,i})/(L_e/D_e)$ of both the thick and thin rods for diameter ratios $d = 2$, 3, and 4, respectively. The phase diagrams of these systems in the $x_2 - \Pi$ representation are shown in Figs. 8(a)–8(c). We begin with a mixture of $x_2 = 0.25$ at low pressure. We then increase $\Pi$, calculating $L_e$ and $D_e$ at each step, until we reach the I-N coexistence regime. We then follow the two coexisting phases until we leave the I-N coexistence regime, entering either a single phase nematic region or a N-N demixing region, depending on the system studied.

For $d = 2$, the phase behavior is relatively straightforward, with only I-N coexistence found. In Fig. 7(a) we see that for the isotropic phase of this system the effective shape of both the thick and the thin rods is about 20% of their actual $L/D$, corresponding to $L_{e,i} \sim 0.6\ L_i$ and $D_{e,i} \sim 3\ D_i$. Entering the I-N coexistence region, we see that the rods in the isotropic phase maintain the same effective shape, while in the nematic phase, the rods stretch out considerably. Interestingly, we see that the thick rods stretch out more than the thin rods, which implies that the system effectively becomes a mixture in length as well as diameter. Upon entering the single phase

nematic region, the rods continue to stretch out as the pressure is increased, the thick rods more so than the thin ones.

As we increase $d$ to 3, which results in increasingly rich phase behavior with the emergence of a N-N demixing regime, we again observe the rods stretching out to different degrees in the coexisting phases (Fig. 7(b)). We see that in the I-N region, the rods in the nematic phase stretch out with increasing pressure before the effective shape reaches a maximum. It then decreases slightly just before the system enters the single phase nematic region, despite the increase in pressure. This corresponds to the coexisting nematic phase becoming increasingly rich in thin rods (and poor in thick rods), with the decrease in the effective shape likely due to the relative decrease in excluded volume interactions associated with this. Thus, the rods are not forced to stretch out as much despite the increase in pressure. A similar effect can also be seen upon entering the N-N coexisting region, where we see that the rods in the thick-rod-rich nematic phase are stretched out more than those in the thin-rod-rich nematic phase.

For mixtures with $d = 4$ (Fig. 7(c)), the rods behave in a similar way to systems with $d = 3$, stretching out in the various nematic phases as the pressure is increased, more so in the nematic phases that are richer in thick rods, and with the thick rods stretched out more than the thin ones. In this system, however, the N-N demixing region begins from an I-N-N triple point, at which we see that the rods in each of the three coexisting phases are stretched out to different degrees. Firstly, in the isotropic phase we, as before, see $L_{e,i}/D_{e,i} \sim 0.2\ L_i/D_i$ for both the thick and thin rods. In the thin-rod-rich nematic phase the rods are considerably more stretched out, with $L_{e,1}/D_{e,1} \sim 0.6\ L_1/D_1$ and $L_{e,2}/D_{e,2} \sim 0.8\ L_2/D_2$. In the thick-rod-rich nematic phase we see $L_{e,1}/D_{e,1} \sim 0.8\, L_1/D_1$ and $L_{e,2}/D_{e,2} \sim 0.9\, L_2/D_2$, giving three phases with three distinct rod behaviors. We thus conclude that any rigid rod treatment of semi-flexible particles, such as the fd-virus, will miss some of the key physics.

### B. Modified thick-thin fd-virus mixtures

Recent progress in the bio-engineering of fd-virus particles allows for tuning their flexibility,[33] and we therefore also apply our model to binary mixtures of fd-virus particles of various persistence lengths. We keep $d$ fixed, and set $L_1 = L_2 = 0.88\ \mu$m and $D_1 = 6.6$ nm in all cases, and calculate the phase diagrams for various $P = P_1 = P_2$ values. In Fig. 9 we show example phase diagrams for $d = 3$ for $P$ ranging from 20 $\mu$m to 0.5 $\mu$m.

As can be seen, the progression of the phase behavior as $P$ is decreased is remarkably similar to that observed when increasing $d$ for the standard fd-virus mixtures with $P = 2.2\ \mu$m. To summarize these results, we divide the ($d$, $P$) plane into regimes featuring different phase diagrams (see Fig. 10), from those where only an I-N transition is found (for stiff rods and small $d$), all the way to complex phase diagrams with I-N, I-I, N-N phase coexistence and I-I-N and I-N-N triple points (for flexible rods and large $d$). We see that increasing $d$ and decreasing $P$ clearly have similar effects on the phase diagram, and hence increasing the flexibility enhances

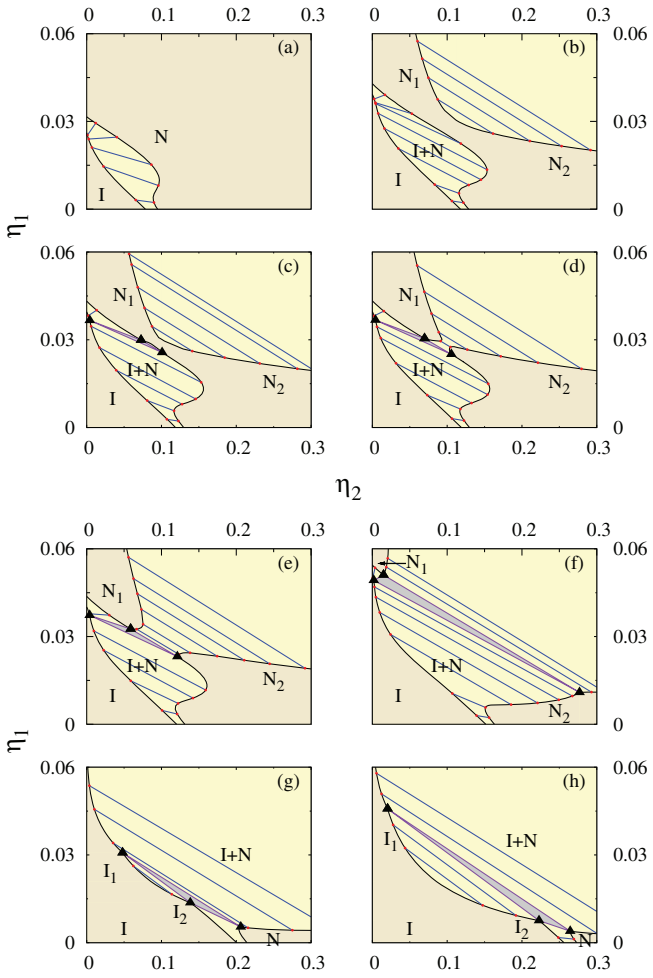


FIG. 9. Phase diagrams for mixtures of modified bare (thin) fd-virus particles (species 1) and PEG-coated (thick) ones (species 2) in the packing fraction representation $\eta_2$–$\eta_1$, with $L_1 = L_2 = 0.88\ \mu$m, $D_1 = 6.6$ nm, $d = D_2/D_1 = 3$, and persistence length $P_1 = P_2 =$ (a) 20 $\mu$m, (b) 1.9 $\mu$m, (c) 1.86 $\mu$m, (d) 1.85 $\mu$m, (e) 1.8 $\mu$m, (f) 1.1 $\mu$m, (f) 0.7 $\mu$m, and (h) 0.5 $\mu$m. The lighter areas indicate the two-phase regions with tie-lines connecting coexisting state-points; triangles denote I-N-N and I-I-N triple points.

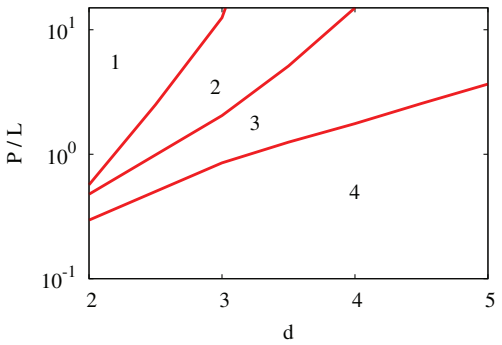


FIG. 10. Topology of the phase diagram (two- and three-phase coexistence) of binary mixtures of (modified) fd-virus particles (see text) as a function of their diameter ratio $d = D_2/D_1$ and persistence length $P = P_1 = P_2$, with fixed $L = L_1 = L_2 = 0.88\,\mu$m and $D_1 = 6.6$ nm. (1) I-N coexistence only. (2) I-N coexistence, N-N demixing beginning from a lower critical point and extending to infinite densities. (3) I-N coexistence, N-N demixing beginning from an I-N-N triple point and extending to infinite densities. (4) I-N coexistence, N-N demixing beginning from an I-N-N triple point and extending to infinite densities, I-I demixing beginning from a lower critical point and ending in an I-I-N triple point.

the complexity of the phase diagrams considerably. This offers increased possibilities for tuning the phase behavior of semi-flexible rod mixtures, through the choice of stiffness and diameter ratio.

### C. Long-short fd-virus mixtures

It is also possible to produce fd-virus particles of different lengths[26,36] and we now study the effects of particle stiffness on long-short fd-virus mixtures of equal diameter. Experimentally, it is possible to produce fd-virus of lengths ranging from $L = 0.3$ $\mu$m to 2 $\mu$m, and with persistence lengths $P = 2.2$ $\mu$m to 10 $\mu$m.[36] Here, we only study the most extreme length ratio case, setting $L_1 = 0.3$ $\mu$m and $L_2 = 2$ $\mu$m to give a length ratio $q = L_2/L_1 = 6.67$, which for rigid rods is known to exhibit I-N coexistence with a N-N demixing region beginning from an I-N-N triple point and extending to infinite densities.[20] We initially fix $P_1 = 2.2$ $\mu$m, and then control the stiffness of the longer rod by varying $P_2$ from 2.2 $\mu$m to 10 $\mu$m. The resulting phase diagrams are shown in Figs. 11(a)–11(g). Figure 11(h) shows the case where $P_1 = P_2 = 10$ $\mu$m with the same length ratio $q = 6.67$. The diameter ratio is kept constant at $d = 1$ in all cases.

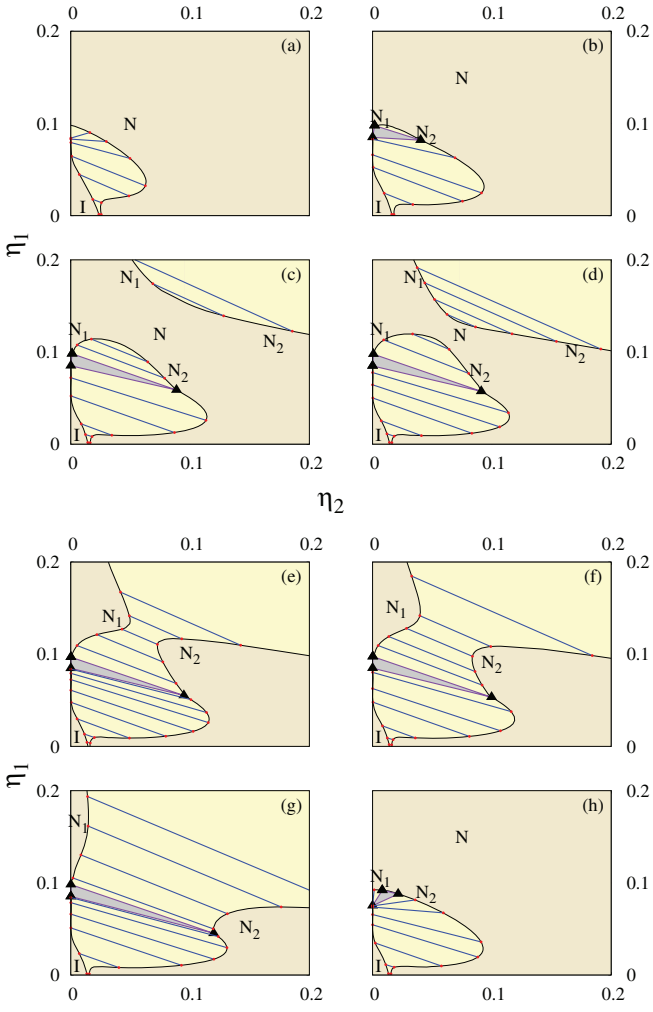


FIG. 11. Phase diagrams for mixtures of short fd-virus particles (species 1, with $L_1 = 0.3$ $\mu$m) and long ones (species 2, with $L_2 = 2$ $\mu$m), with length ratio $q = 6.67$ and diameter ratio $d = 1$, in the $\eta_2$–$\eta_1$ representation, with persistence length $P_1 = 2.2$ $\mu$m and $P_2 =$ (a) 2.2 $\mu$m, (b) 5 $\mu$m, (c) 7.5 $\mu$m, (d) 7.6 $\mu$m, (e) 7.8 $\mu$m, (f) 8 $\mu$m, and (g) 10 $\mu$m. (h) $P_1 = P_2 = 10$ $\mu$m. The lighter areas indicate the two-phase regions with tie-lines connecting coexisting state-points; triangles denote I-N-N and I-I-N triple points.

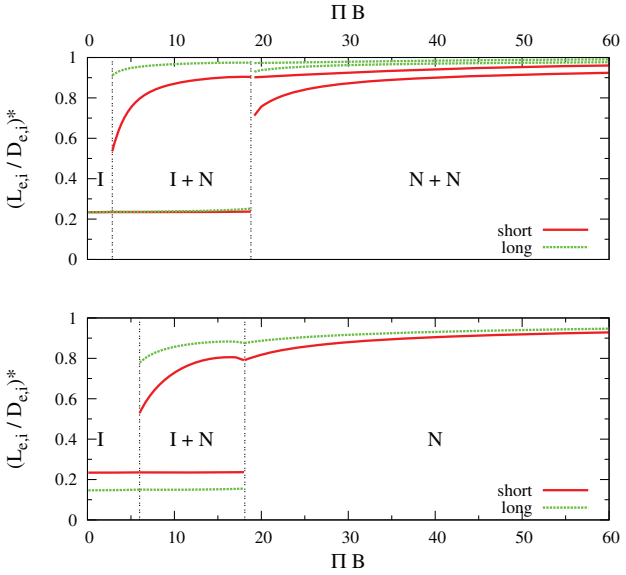


FIG. 12. Effective shape $L_{e,i}/D_{e,i}$ of short (solid line) and long (dashed line) fd-virus of $d = 1$ and length ratio $q = L_2/L_1 = 6.67$ as a function of osmotic pressure $\Pi$, beginning from an initial long-rod mole fraction of $x_2 = 0.05$. Solid line indicates actual length and diameter ratios. The top plot shows the case where $P_2 = 10$ $\mu$m, while the right plot shows the case where $P_2 = 2.2$ $\mu$m. In all cases $P_1 = 2.2$ $\mu$m.

At low $P_2$ values, we find only I-N coexistence in the density regime of interest (Fig. 11(a)), with some degree of fractionation. Increasing $P_2$ results in a greater degree of fractionation and the emergence of a N-N coexistence regime (shown in Fig. 11(b)). This begins from an I-N-N triple point, and ends in an upper critical point. We find this behavior to begin at $P_2 \sim 4$ $\mu$m, while in rigid rod mixtures, such phase behavior has been reported for length ratios greater than $\sim$3.[20] Further increasing $P_2$ to about $\sim$7 $\mu$m results in the emergence of a second N-N coexistence regime (in the density region of interest), which begins from a lower critical point (this behavior is shown in Fig. 11(c) for $P_2 = 7.5$ $\mu$m). As $P_2$ is increased further, the two N-N regimes become larger (Fig. 11(d)), until they merge to form a single N-N coexistence region (shown in Fig. 11(e)). We find this behavior to begin at about $P_2 = 7.7$ $\mu$m, and for $P_2$ larger than this, the N-N region shows increasing fractionation. In rigid rod mixtures such phase diagrams are found for length ratios beyond $\sim$3.2.[20]

This change in phase behavior is due to the change in the effective shape of the longer rod as the stiffness is changed. Figure 12 shows the difference in the effective shape throughout the phase diagram for the two most extreme systems, $P_2 = 10$ $\mu$m and $P_2 = 2.2$ $\mu$m (again with $L_1 = 0.3$ $\mu$m and $L_2 = 2$ $\mu$m). Here, we begin with a mixture of $x_2 = 0.05$ in the single phase isotropic region, and increase the osmotic pressure $\Pi$. As can be seen, while the behavior of the short rods is very similar between the two systems, the long rods behave much differently, particularly in the isotropic phase where for

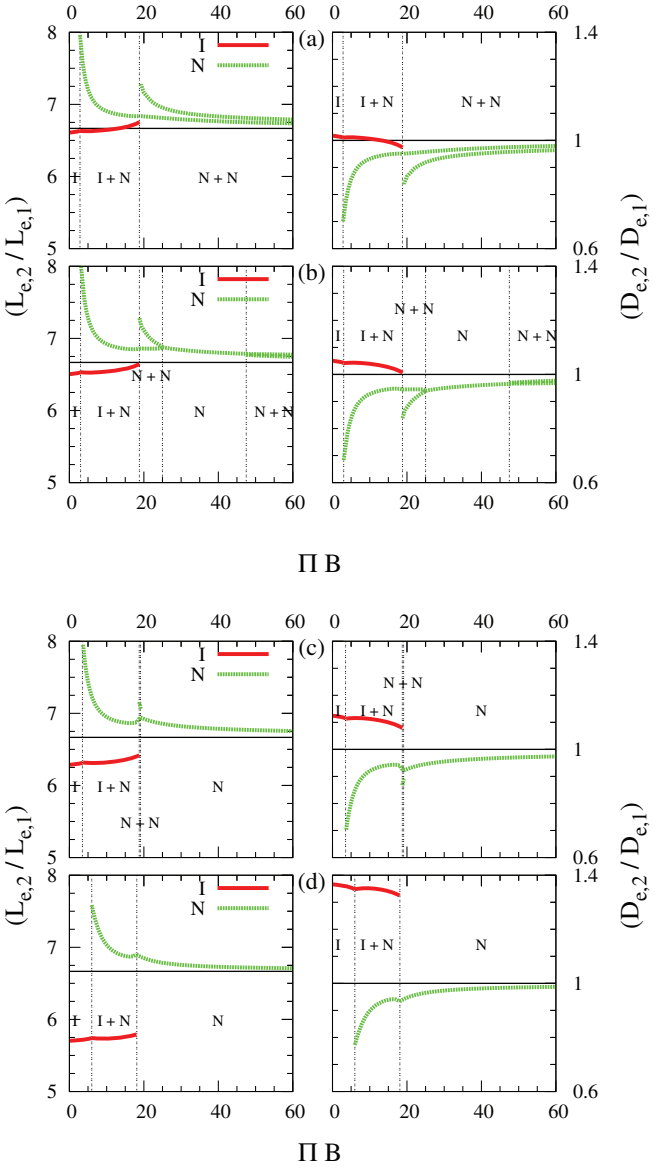


FIG. 13. Effective length ratio $L_{e,2}/L_{e,1}$ and diameter ratio $D_{e,2}/D_{e,1}$ of long-short fd-virus mixtures of length ratio $q = L_2/L_1 = 6.67$ and diameter ratio $d = 1$ as a function of osmotic pressure Π, beginning from an initial long rod mole fraction of $x_2 = 0.05$. (a) $P_2 = 10$ $\mu$m, (b) $P_2 = 7.5$ $\mu$m, (c) $P_2 = 5$ $\mu$m, and (d) $P_2 = 2.2$ $\mu$m. In all cases $P_1 = 2.2$ $\mu$m. Solid lines show isotropic phases, dashed lines show nematic phases. The actual size ratios are indicated by the horizontal line.

low $P_2$ the long rods stretch out relatively less than the short ones, while for large $P_2$ they show a similar degree of stretching to the short ones. In the nematic phase the long rods are always stretched out more regardless of their stiffness.

We now examine the effective size ratios of the rods, shown in Figs. 13(a)–13(d), where we plot the effective length and diameter ratios of several of the systems throughout the phase diagrams, again beginning in the single phase isotropic region with a mixture of $x_2 = 0.05$, and increasing the osmotic pressure Π. In all cases, except that with the largest $P_2$, we see that the effective length ratio is smaller than the actual ratio in the isotropic phase, while the effective diameter ratio is larger than the actual ratio. In the nematic phase the opposite is true, with a larger effective length ratio and smaller effective diameter ratio than the actual values. This gives an indication as to how the phase behavior is controlled: by increasing the stiffness of the longer rod we increase the effective length ratio, which leads to richer phase behavior. As this also decreases the effective diameter ratio, which for a fixed length ratio would lead to less rich phase behavior but here leads to richer behavior, we may infer that length ratio plays a more dominant role in determining phase behavior than diameter ratio. This should not come as a surprise if one realizes that the excluded volume of rods as given in Eqs. (4) and (24) is linear in the diameter and quadratic in the lengths. We also note that the biggest difference between the behavior of the effective size ratios of the rods is in the isotropic phase.

While increasing the stiffness of the long rod for a fixed short rod stiffness leads to increasingly rich phase behavior, we find the opposite effect when increasing the stiffness of the short rod for a fixed long rod stiffness. Figure 11(h) shows the phase diagram for a long-short mixture, again with $L_1 = 0.3$ $\mu$m and $L_2 = 2$ $\mu$m, with $P_1 = 10$ $\mu$m and $P_2 = 10$ $\mu$m. As can be seen, the phase behavior has now become less rich, with only I-N coexistence and a small N-N demixing regime (beginning from an I-N-N triple point) found. In Fig. 14 we show the effective length and diameter ratios of this system. We see that both the phase diagram itself and the effective shape ratios are remarkably similar to those found for the mixture with $P_1 = 2.2$ $\mu$m and $P_2 = 5$ $\mu$m (shown in Figs. 11(b) and 13(c)), which shows identical phase behavior. To summarize these results, we divide the $(P_1, P_2)$ plane into regions featuring different phase diagrams (see Fig. 15), from those where the phase diagrams show only I-N coexistence, to those where I-N, I-N-N, and N-N coexistence is found. From this, we see that increasing the stiffness of the long rod (for a fixed short rod stiffness) has the same effect on phase behavior as decreasing the short rod stiffness (for a fixed long rod stiffness). While we have only studied one length ratio here, we would expect to see the same basic behavior for other ratios, with the diagram shown in Fig. 15 showing either a larger rich phase behavior region (for larger length ratios) or a smaller one (for smaller length ratios).

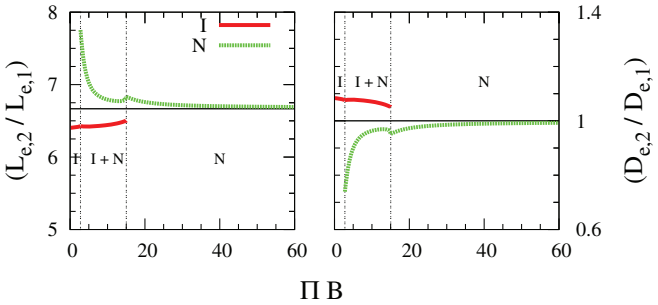


FIG. 14. Effective length ratio $L_{e,2}/L_{e,1}$ and diameter ratio $D_{e,2}/D_{e,1}$ of long-short fd-virus mixtures with $P_1 = 10$ $\mu$m and $P_2 = 10$ $\mu$m, length ratio $q = L_2/L_1 = 6.67$, and diameter ratio $d = 1$ as a function of osmotic pressure Π, beginning from an initial long rod mole fraction of $x_2 = 0.05$. Solid lines show isotropic phases, dashed lines show nematic phases. The actual size ratios are indicated by the horizontal line.

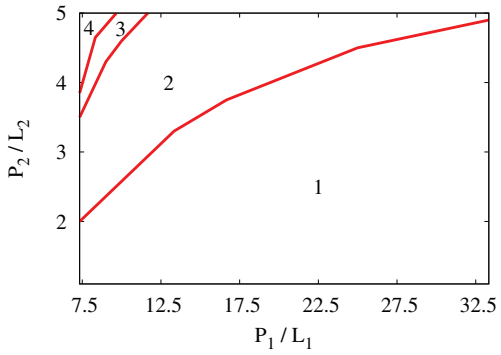


FIG. 15. Topology of the phase diagram (two- and three-phase coexistence) of long-short binary mixtures of (modified) fd-virus particles (see text) as a function of the persistence lengths $P_1$ and $P_2$, with fixed $L_1 = 0.3$ $\mu$m and $L_2 = 2$ $\mu$m ($q = 6.67$), and $D_1 = D_2 = 6.6$ nm ($d = 1$). (1) I-N coexistence only. (2) I-N coexistence, N-N demixing beginning from an I-N-N triple point and ending in an upper critical point. (3) I-N coexistence, N-N demixing beginning from an I-N-N triple point and ending in an upper critical point, N-N demixing beginning from a lower critical point and extending to infinite densities. (4) I-N coexistence, N-N demixing beginning from an I-N-N triple point and extending to infinite densities.

## V. CONCLUSIONS

In this paper, we have presented a theoretical model to describe suspensions of semi-flexible colloidal rods, which we have applied here to fd-virus particles. We have studied the influence of the geometry and stiffness of the virus particles on the behavior of a range of systems. For monodisperse systems, we find that, in agreement with previous studies, isotropic-nematic coexistence is moved to significantly higher densities as the rods are made more flexible, with the increase in flexibility causing the first-order transition to become increasingly weaker. We have also calculated the nematic order parameter along the length of the rods, finding them to be more aligned in the center than the ends, particularly for more flexible particles. At densities just above the I-N coexistence density the nematic ordering changes continuously along the contour, reaching a peak value in the center. At higher densities we see the peak value in the center become a plateau and that the less ordered end sections become shorter. We have also calculated the effective shape of the rods in both the isotropic and nematic phases. We find the effective aspect ratio to be always much smaller than the actual shape for all but the stiffest rods studied, particularly in the isotropic phase, with persistence lengths much larger than those that are possible to produce experimentally for fd-virus particles required for the rods to be considered effectively rigid. Indeed, it seems that the excluded volume induced stretching of the rods in the nematic phase has a greater effect in stretching out fd-virus particles than increasing the persistence length, with the most flexible particles studied here having a larger effective shape in the nematic phase than all but the stiffest rods have in the isotropic phase.

We have also studied thick-thin binary mixtures of fd-virus particles. Consistent with experimental observations we find I-N, N-N, and I-N-N coexistence, as well as I-I and I-I-N coexistence at diameter ratios larger than those studied in experiments so far. Our results also show good quantitative agreement with experimental data. We find that the effective shape of the rods changes widely throughout the systems studied, with the thick rods stretching out more than the thin rods. Interestingly, we find that the rods stretch out more in nematic phases that are richer in thick rods than thin ones, showing the effects of the larger excluded volume interactions in these phases on the stretching of semi-flexible rods. We also see that altering the stiffness of the fd-virus particles has the same effect on phase behavior as changing the diameter ratio, with a decrease in particle stiffness leading to increasingly rich phase behavior.

Finally, we have studied long-short binary mixtures consisting of fd-virus particles of identical diameter and differing persistence and contour lengths. We find the richest phase behavior for systems consisting of stiffer long rods and more flexible short rods. Decreasing the stiffness of the long rods or increasing that of the short rods results in less rich phase behavior. This is despite the fact that the length ratio we studied shows very rich phase behavior in rigid rod systems, and that the persistence lengths we study are always larger than the contour lengths of the rods. The reason for this lies in the effective length ratio, which is largest for systems comprising of stiff long rods and more flexible short rods, and can be used to control the phase behavior. We find that the effective diameter ratio, which is larger for smaller effective length ratios, appears to play a less significant role in influencing phase behavior.

In conclusion, we find the behavior of fd-virus systems to be very sensitive to the stiffness of the constituent particles, with only small changes in particle stiffness required to give dramatic changes in the observed phase behavior. This gives an enhanced degree of control over phase behavior, with the possibility to, say, control the degree of fractionation in coexisting phases, important for purifying samples. In future work we aim to study further the interplay between the stiffness and length of semi-flexible rods and the resultant particle behavior. We hope that this work stimulates further experimental studies of bio-engineered fd-virus suspensions and other semi-flexible particles.

## ACKNOWLEDGMENTS

Z. Dogic is acknowledged for useful discussions on fd-virus engineering. This work is financed by a NWO-VICI grant and is part of the research program of the "Stichting door Fundamenteel Onderzoek der Materie (FOM)" which is financially supported by the "Nederlandse organisatie voor Wetenschappelijk Onderzoek (NWO)."

[1] L. Onsager, Ann. N.Y. Acad. Sci. **51**, 627 (1949).
[2] B. M. Mulder and D. Frenkel, Mol. Phys. **55**, 1193 (1985).
[3] A. Samborski and G. T. Evans, J. Chem. Phys. **93**, 4254 (1990).
[4] A. Samborski, G. T. Evans, C. P. Mason, and M. P. Allen, Mol. Phys. **81**, 263 (1994).
[5] P. D. Duncan, M. Dennison, A. J. Masters, and M. R. Wilson, Phys. Rev. E **79**, 031702 (2009).
[6] A. R. Khokhlov and A. N. Semenov, Physica A **108**, 546 (1981).
[7] A. R. Khokhlov and A. N. Semenov, Physica A **112**, 605 (1982).
[8] M. Dijkstra and D. Frenkel, Phys. Rev. E **51**, 5891 (1995).
[9] Z. Y. Chen, Macromolecules **26**, 3419 (1993).
[10] G. T. Evans, J. Chem. Phys **104**, 6654 (1996).

[11]T. Odijk, Macromolecules **19**, 2313 (1986).
[12]P. P. F. Wessels and B. M. Mulder, Soft Mater. **1**, 313 (2003).
[13]P. P. F. Wessels and B. M. Mulder, J. Phys. Condens. Matter **18**, 9335 (2006).
[14]M. Dennison, M. Dijkstra, and R. van Roij, Phys. Rev. Lett. **51**, 627 (2011).
[15]G. J. Vroege and H. N. W. Lekkerkerker, J. Phys. Chem. **97**, 3601 (1993).
[16]R. van Roij, B. Mulder, and M. Dijkstra, Physica A **261**, 374 (1998).
[17]M. Dijkstra and R. van Roij, Phys. Rev. E **56**, 5594 (1997).
[18]H. N. W. Lekkerkerker, P. Coulon, R. van der Haegen, and R. Deblieck, J. Chem. Phys. **80**, 3427 (1984).
[19]T. Odijk and H. N. W. Lekkerkerker, J. Phys. Chem. **89**, 2090 (1985).
[20]R. van Roij and B. Mulder, J. Chem. Phys. **105**, 11237 (1996).
[21]H. H. Wensink and G. J. Vroege, J. Phys.: Condens. Matter **16**, S2015 (2004).
[22]P. A. Buining and H. N. W. Lekkerkerker, J. Phys. Chem. **97**, 11510 (1993).
[23]T. Sato, N. Ikeda, T. Itou, and A. Teramoto, Polymer **30**, 311 (1989).
[24]K. R. Purdy, S. Varga, A. Galindo, G. Jackson, and S. Fraden, Phys. Rev. Lett. **94**, 057801 (2005).
[25]J. Tang and S. Fraden, Liq. Cryst. **19**, 459 (1995).
[26]Z. Dogic and S. Fraden, Philos. Trans. R. Soc. London, Ser. A **359**, 997 (2001).
[27]E. Grelet, Phys. Rev. Lett. **100**, 168301 (2008).
[28]J. D. Parsons, Phys. Rev. A **19**, 1225 (1979).
[29]S. D. Lee, J. Chem. Phys. **87**, 4972 (1987).
[30]S. Varga, K. R. Purdy, A. Galindo, S. Fraden, and G. Jackson, Phys. Rev. E **72**, 051704 (2005).
[31]H. Fynewever and A. Yethiraj, J. Chem. Phys. **108**, 1636 (1998).
[32]A. N. Semenov and A. V. Subbotin, Polym. Sci. USSR **31**, 2266 (1989).
[33]E. Barry, D. Beller, and Z. Dogic, Soft Matter **5**, 2563 (2009).
[34]G. J. Vroege and H. N. W. Lekkerkerker, Rep. Prog. Phys. **55**, 1241 (1992).
[35]R. van Roij, Eur. J. Phys. **26**, S57 (2005).
[36]Z. Dogic, personal communication (1 March 2011).